Effects of Short Diblocks at Interfaces of Strongly Segregated Long Diblocks

An-Chang Shi* and Jaan Noolandi*

Xerox Research Centre of Canada, 2660 Speakman Drive, Mississauga, Ontario, Canada L5K 2L1

*Received November 29, 1993; Revised Manuscript Received March 7, 1994**

ABSTRACT: Mixtures of small amounts of short diblocks (cosurfactants) and chemically identical large diblocks (surfactants) are considered, when the large diblocks are in the strongly segregated regime. Due to the enthalpy gain, the short diblocks segregate to the interfaces and change the interfacial properties. The competition between the interfacial free energy reduction and the packing free energy change determines the phase behavior of the system. It is shown that large changes can be expected in the global phase diagram when both short and long chain composition ratios are varied. At some places on the phase boundaries between structures of different symmetries the increase in the packing free energy density corresponding to the addition of nearly symmetrical short diblocks cancels the reduction in the interfacial free energy density, and varying the concentration of small chains has no effect on the stability of the phases in the vicinity of these structural fixed points. Elsewhere, large changes in the stabilities of phases of different symmetries can occur depending on the composition ratios of the short and long copolymers, and whether the short molecules behave as compatibilizers at the domain boundaries or act more like homopolymer fillers in the bulk domains. Density profiles of both large and short diblocks, based on mean-field calculations, are presented.

1. Introduction

Block copolymer phase behavior has been studied extensively over the past years.[1] The observed morphologies have been correlated with monomer types, molecular architectures, compositions, and molecular sizes. For diblocks of polystyrene and polyisoprene the influence of solvent on the order–disorder transition, and on the ordered-phase symmetries, has been discussed in detail by Hashimoto and co-workers.[2] Theories of ordered microstructures deal primarily with the delicate balance between the packing and interfacial free energies and analyze how this balance is related to structural features such as the interfacial curvature. There are still some outstanding problems to be solved in this area, one of them being the stability of the ordered bicontinuous double-diamond (OBDD) phase.[3,4]

For a fixed chemical composition of a diblock copolymer the only variables left are the block sizes, which means there is a limited range of morphological behavior which can be observed for such a system (we do not consider here solvent in the final state of the equilibrium system, because of the complications of dealing with a different chemical component). On the theoretical side, once the chemical composition of such a system is fixed, there is a well-defined relation at thermodynamic equilibrium between the packing and interfacial free energies, involving the interfacial curvature. In this paper we consider systems in which this relation can be altered by external means, so as to widen the range of observed morphological behavior and to test and refine theoretical concepts for analyzing the structural stability of these systems.

Short diblocks (cosurfactants) which have the same chemical structure, but a different composition from the large diblocks (surfactants), are considered to be added to large diblocks in small amounts. This decouples the interfacial free energy of an ordered large diblock system from the packing free energy only partially, as will be shown later. Since the composition of the short diblocks can be different from that of the long diblocks, one important effect of the short diblocks at the domain boundaries is on the interfacial curvature, which has implications for the stability of phases of different symmetries. We have performed detailed mean-field calculations of the distribution functions, density profiles, and associated free energy densities for the mixed and pure diblock systems. A schematic diagram of known diblock morphologies with a short diblock "hairy" interface is shown in Figure 1. Note that the equilibrium phase boundaries have been shifted from the values for a "clean" interface, for the molecular parameters indicated. It is not known at present whether new ordered-phase symmetries with lower free energies are possible for these surfactant–cosurfactant systems. Our model calculations have all been carried out for existing symmetries, leaving out the OBDD phase. In section 2 we discuss the free energy for the mixed system, and section 3 contains the polymer density and end-distribution profiles for various cases. In section 4 we conclude with discussions on the results, and the Appendix contains the details of the mean-field calculations.

2. Free Energy of Short Diblock–Long Diblock Mixtures

We will consider systems for which a few volume percent of short diblocks (with $\chi Z_s < 10.5$) have been added to a system of large diblocks (with $\chi Z_l \gg 10.5$), where χ is the Flory–Huggins interaction parameter, and Z_l and Z_s are the degrees of polymerization of the long and short diblock copolymer chains, respectively. The short diblocks are not able to form an ordered phase by themselves, and the large diblocks are in the strongly segregated regime. Both short and long diblocks are composed of A and B units, and the fractions of A units in the short and long molecules are denoted by f_s and f_l, respectively. We assume that χ is independent of chain length, and when there is a system of A–B blocks with chains of different lengths and asymmetries, one χ is sufficient to represent all interactions.

Short diblocks are added to the long diblocks in the high-temperature disordered phase, possibly with the assistance of an almost nonselective solvent to ensure homogeneous mixing. This process incurs a free energy (density) cost of f_{mix}. The solvent is then evaporated, and

* Abstract published in *Advance ACS Abstracts*, April 15, 1994.

0024-9297/94/2227-2936$04.50/0

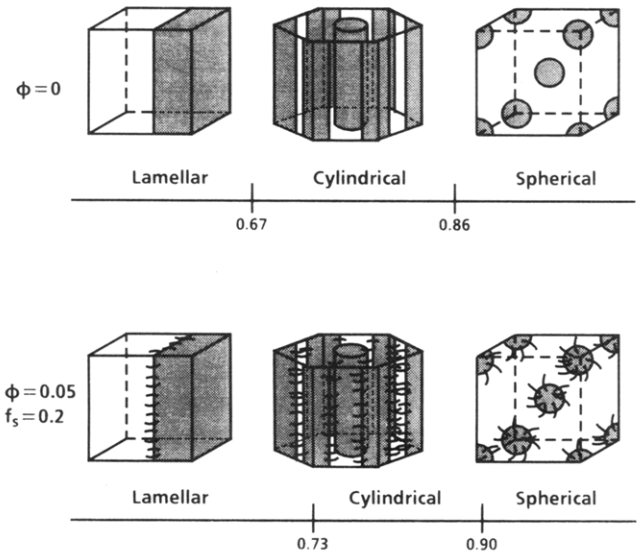

Figure 1. Block copolymer morphologies with a clean interface (top) and a "hairy" interface (bottom). The phase boundaries are calculated for $Z_l = 500$, $Z_s = 50$, and $\chi = 0.2$. ϕ is the volume fraction of short diblock copolymers. f_l is the composition fraction of A units in the long AB diblocks, and $f_s = 0.2$ is the corresponding composition fraction for the short AB diblocks.

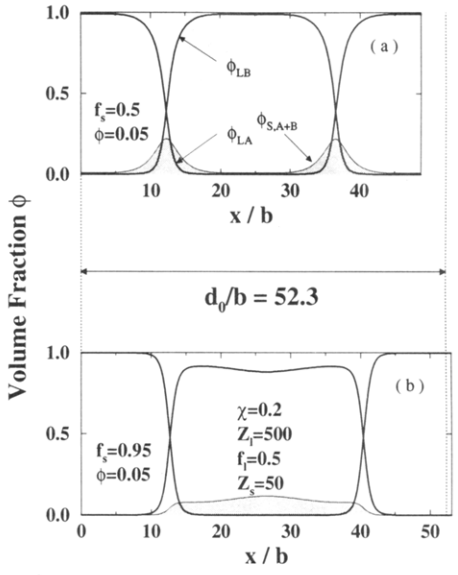

Figure 2. Calculated lamellar concentration profiles for $Z_l = 500$, $Z_s = 50$, $f_l = 0.5$, and $\phi = 0.05$ for (a) $f_s = 0.5$ and (b) $f_s = 0.95$. The long chain profiles are plotted as solid lines, and the short chain profiles are represented by the shaded areas. The equilibrium domain spacing of the pure diblock system (d_0) is indicated in the middle. For symmetric short diblocks (top panel) the small molecules localize at the interfaces. For asymmetric short diblocks (bottom panel) the small molecules localize in the domains. All distances are expressed in terms of the Kuhn's length b.

the temperature is lowered, causing the long diblocks to form a periodic array of amorphous domains. The small diblocks are trapped in the large domains of the ordered mesophase and establish an equilibrium whereby their chemical potential is the same in all the domains. Some of the short diblocks locate at the domain boundaries for energetic reasons, in much the same way that large diblocks locate at the interface between homopolymers in their role as compatibilizers.[5] Some of the free energy cost of mixing the short diblocks into the large diblocks is thereby recovered. The remainder of the short diblocks are distributed in the bulk of the domains of the mesophase. The behavior of the short diblocks depends on their composition f_s. When the lengths of the A and B blocks of the short chains are comparable ($f_s \sim 0.5$), the short diblocks segregate to the interfaces and behave as compatibilizers. When the short chains are highly asymmetric ($f_s \sim 0$ or 1), most of the short diblocks are localized in their corresponding bulk domains and act like homopolymer fillers. This different behavior is demonstrated in Figure 2, where the calculated polymer density profiles for $f_s = 0.5$ and 0.95 are given. The localization of the short diblocks at the interfaces for $f_s = 0.5$ (Figure 2a) and in the domains for $f_s = 0.95$ (Figure 2b) is evident. The different short chain behaviors have different effects on the phase behavior of the system.

Consider for the moment the large diblock system without short diblocks. Following the usual rationale for the formation of ordered domains in the low-temperature regime, the incompatible A and B blocks are able to avoid each other, allowing for a large reduction in the interaction energy except at the domain boundaries, where the A and B blocks of the copolymers are joined.[6] The domain boundary free energy is usually expressed in terms of the interfacial tension (interfacial free energy per unit area). The formation of the ordered phase takes place in such a way that the interfacial energy per unit volume is reduced as much as possible, limited by the stretching free energy of the blocks necessary to maintain a constant packing density throughout the domains. The symmetry of the ordered phase depends on the interaction energy of the blocks as well as the relative block lengths. The free energy density of the ordered lamellar phase (relative to the disordered phase) can be written approximately as

$$f = f_0 + \gamma_0/d + C_0 d^{\alpha} \tag{1}$$

where f_0 is the demixing free energy of the A and B blocks relative to the disordered phase, γ_0 is the surface tension of the domain boundary interface, C_0 is a function of the block lengths, d is the domain size (*i.e.*, distance between neighboring domain centers), and α is a phenomenological exponent which varies from about 2.5[7] to the exact value of 2.0 (for very large Z_A[8]) in the strongly segregated region. Similar expressions are available for phases of different symmetries.[9,10] Minimizing the free energy density with respect to d gives the equilibrium domain size. When small amounts of short symmetric diblocks are added to the large diblocks (following the process described earlier), the domain boundary interfacial tension is reduced, as noted before. The packing free energy is changed, however, since some of the long diblock copolymers with their joints located at the domain boundaries are replaced by short diblocks and the smaller number of long diblocks as well as the short diblocks must rearrange themselves to maintain a constant packing density in the bulk of the domains. The free energy density of the long diblocks with a small amount of added short diblocks can then be written to first order in the short diblock volume fraction as

$$f = f_0 + f_{mix} + (\gamma_0 - \Delta\gamma\phi)/d + (C_0 + C_1\phi)d^{\alpha} \tag{2}$$

where ϕ is the volume fraction of short diblocks, $-\Delta\gamma\phi$ is the reduction in the interfacial tension arising from the interaction energy reduction corresponding to the localization of some of the short diblocks at the domain boundary interface, $C_1\phi d^{\alpha}$ is the change in the stretching free energy of the long diblocks and short diblocks required to maintain a constant packing density, and f_{mix} is the free energy increase associated with the mixing of the short diblocks into the long diblock domains. It should be noted

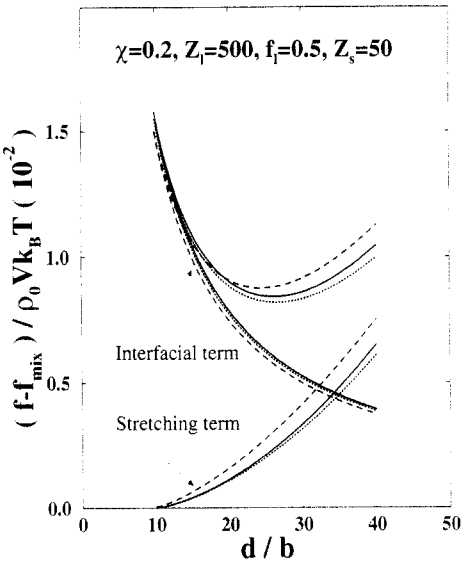

Figure 3. Calculated free energies for $\chi = 0.2$, $Z_l = 500$, $Z_s = 50$, $f_l = 0.5$, and $\phi = 0.05$. The solid lines are for the pure diblocks; dashed lines ($f_s = 0.5$) and dotted lines ($f_s = 0.95$) are with added short chains. The interfacial ($\propto d^{-1}$) and entropic ($\propto d^{\alpha}$) contributions are shown. The mixing free energy of the short diblocks is omitted in the figure. The domain spacing is scaled by the Kuhn's length b, which is put equal to unity in the calculations. For approximately symmetric short diblocks (cosurfactants) the domain spacing decreases, whereas for very asymmetric short diblocks (fillers) the domain spacing increases.

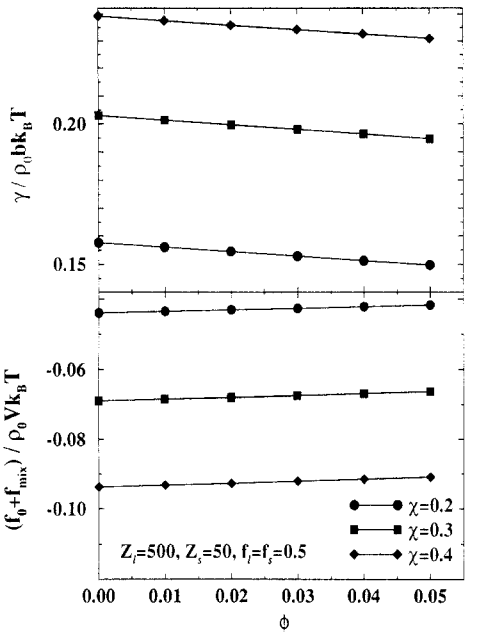

Figure 4. Interfacial tension and free energies of mixing for increasing short diblock volume fractions.

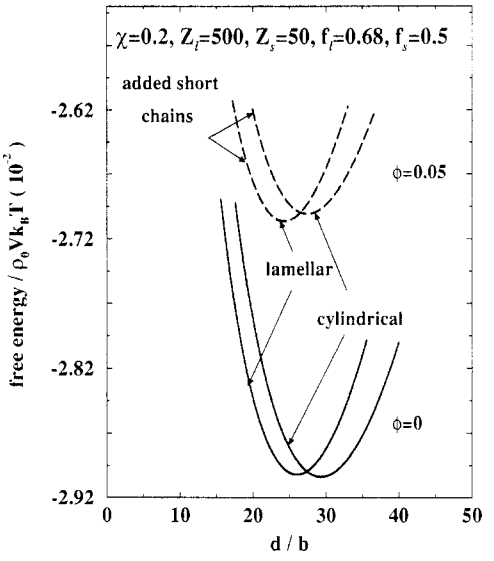

Figure 5. Free energies for lamellar and cylindrical phases, with and without short diblocks, close to the clean interface phase boundary.

that the stretching term $C_1\phi d^{\alpha}$ can be positive or negative, depending on whether the short diblocks act as compatibilizers (symmetric) or fillers (asymmetric). In order to focus on the relevant physics we note that for small d the free energy must scale inversely with d because the interfacial free energy per unit volume is the dominant term. Knowing the functional form of the free energy for small d allows us to determine the coefficient for the interfacial tension term and extending this contribution to larger d we obtain the entropic stretching term by subtraction. As expected, for large d the entropic stretching term dominates the free energy. The decomposition of the total free energy with and without short diblocks into the physically interesting contributions is shown in Figure 3 for $\chi = 0.2$, $Z_l = 500$, $Z_s = 50$, $\phi = 0.05$, $f_l = 0.5$, and $f_s = 0.5$ and 0.95. The lowering of the interfacial tension as well as the change in the stretching energy of the long diblocks with added short diblocks is evident, and we have not shown the mixing free energy when the short diblocks are present. For the symmetric short diblocks ($f_s = 0.5$), there is a decrease in the interfacial tension and an increase of the stretching energy, resulting in a decrease of the equilibrium domain size. For the highly asymmetric short diblocks ($f_s = 0.95$), there is little change in the interfacial tension and a decrease in the stretching energy, resulting in an increase of the equilibrium domain size. Figure 4 shows the decrease in the interfacial tension and the increase in the mixing free energy with increasing volume fraction of the symmetric short diblocks. The lines showing the interfacial tension reductions for different χ's are approximately parallel. This can be understood by noting that, for a flat interface and equal block lengths, ignoring the entropic terms, the interfacial tension is given approximately by[5]

$$\gamma \simeq \gamma_0 - \frac{d\chi}{2}[\phi_s(0) - \phi_{bulk}] \qquad (3)$$

where d is the interfacial width, $\phi_s(0)$ is the volume fraction of the short diblocks at the interface, and ϕ_{bulk} is the corresponding volume fraction in the domains. Since $\gamma_0 \sim \chi^{1/2}$, $d \sim \chi^{-1/2}$, and $[\phi_s(0) - \phi_{bulk}] \propto \phi$ for small ϕ, we have an almost parallel shift of the lines for χ's in the range 0.2–0.4.

Figure 5 shows that the relative stability of ordered phases of different symmetries can also be affected by the addition of small amounts of short diblocks. Referring to eq 2, the change in the free energy which depends on the domain size is

$$\Delta f(d) = -\Delta\gamma\phi/d + C_1\phi d^{\alpha} \qquad (4)$$

When the two terms in eq 4 do not cancel, the domain size can decrease or increase, depending on whether the short diblocks act as cosurfactants or fillers, as shown in Figure 3. In addition, the relative stabilities of two phases with different symmetries but sufficiently close free energies can be changed, as shown in Figure 5. When the two terms in eq 4 cancel, there are several cases to be considered. If the system is not close to a phase boundary and a phase with a different symmetry does not have a lower free

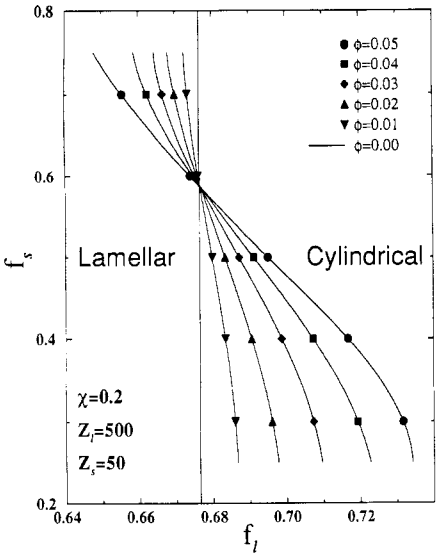

Figure 6. Detail of phase diagram around structural fixed point for different amounts of added short diblocks.

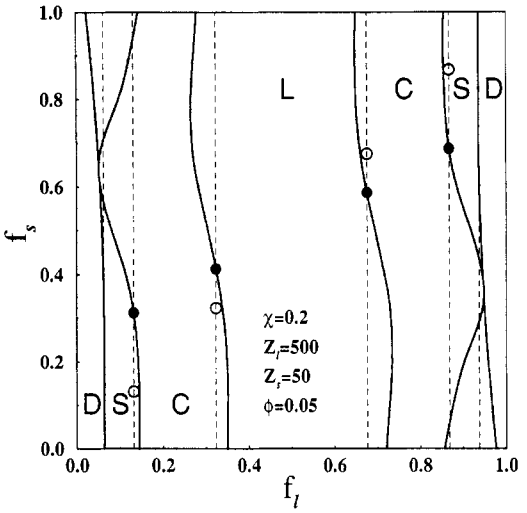

Figure 7. Two-dimensional phase diagram for $\phi = 0.05$ showing structural fixed points (solid circles). The fixed points on the spherical-disordered (S-D) boundaries are not shown as their vertical position is poorly defined because of the shallow crossing of the perturbed and unperturbed lines. The open circles show the positions of the exact points for $Z_s = Z_l$, for which $f_s = f_l$, corresponding to the pure diblock melt.

energy, the addition of the short diblocks causes no structural change, and the domain size is unaffected. If the system is at a phase boundary, the free energies of the phases of different symmetries are individually unaffected, resulting in a structural fixed point. This situation is shown in Figure 6 for the lamellar-cylindrical phase boundary. For $f_s \simeq 0.59$ and $f_l \simeq 0.67$ the stabilities of lamellar and cylindrical phases are unaffected by the addition of small amounts of the short diblock copolymer. Moving away from the fixed point results in large changes in the phase boundary which depend on the amount of added short diblock copolymer. It should be noted that for the case $Z_s = Z_l$, the structural fixed point at $f_s = f_l \simeq 0.67$ is exact in the sense that the conditions $Z_s = Z_l$ and $f_s = f_l$ correspond to a pure diblock copolymer melt. A global phase diagram is shown in Figure 7. In these calculations the ordered double-diamond structure has been ignored, because of the difficulty of calculating the relative stability of this phase. Figure 7 shows a number of structural fixed points (the filled circles) for the different phase boundaries. The fixed points for the case $Z_s = Z_l$ are shown by the open circles. Figure 8 shows the changes

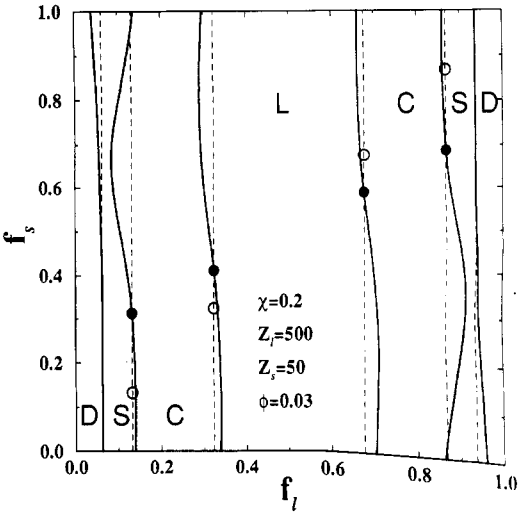

Figure 8. Two-dimensional phase diagram for $\phi = 0.03$ showing structural fixed points (solid circles). The fixed points on the spherical-disordered (S-D) boundaries are not shown as their vertical position is poorly defined because of the shallow crossing of the perturbed and unperturbed lines. The open circles show the positions of the exact fixed points for $Z_s = Z_l$, for which $f_s = f_l$, corresponding to the pure diblock melt.

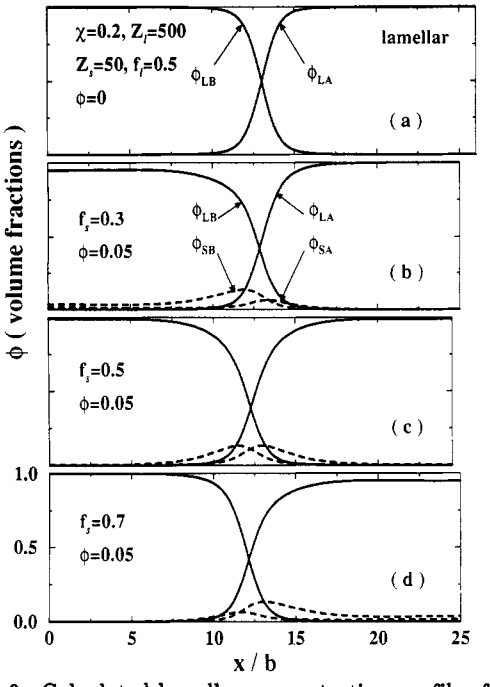

Figure 9. Calculated lamellar concentration profiles for $Z_l = 500$, $Z_s = 50$, and $f_l = 0.5$; (a) $\phi = 0$, (b) $\phi = 0.05$, $f_s = 0.3$, (c) $\phi = 0.05$, $f_s = 0.5$, and (d) $\phi = 0.05$, $f_s = 0.7$. The long chain profiles are plotted as solid lines, and the short chain profiles are plotted as dashed lines. Changes in the lengths of the horizontal axes correspond to the changes in the domain size with added short chains.

in the global phase diagram when the volume fraction of short diblock copolymer is reduced to $\phi = 0.03$. We note that the phase diagrams are symmetric under the transformations $f_l \rightarrow 1 - f_l$ and $f_s \rightarrow 1 - f_s$.

3. Density and End and Joint Distribution Profiles

Figures 9–11 show the density profiles as well as the end and joint distribution functions for a symmetric lamellar structure with $Z_l = 500$, $f_l = 0.5$, and $\chi = 0.2$. The short diblocks are characterized by $Z_s = 50$ and by different composition ratios f_s. The horizontal axis spans the distance from the middle of one domain to the middle of

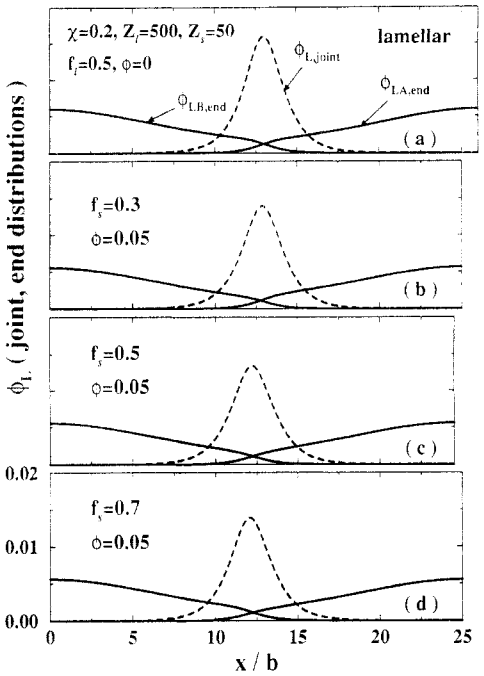

Figure 10. Calculated lamellar joint and end distributions of the long diblocks for $Z_l = 500$, $Z_s = 50$, and $f_l = 0.5$: (a) $\phi = 0$, (b) $\phi = 0.05$, $f_s = 0.3$, (c) $\phi = 0.05$, $f_s = 0.5$, and (d) $\phi = 0.05$, $f_s = 0.7$. The end distributions are plotted as solid lines, and the joint distribution is plotted as dashed lines. Changes in the lengths of the horizontal axes correspond to the changes in the domain size with added short chains.

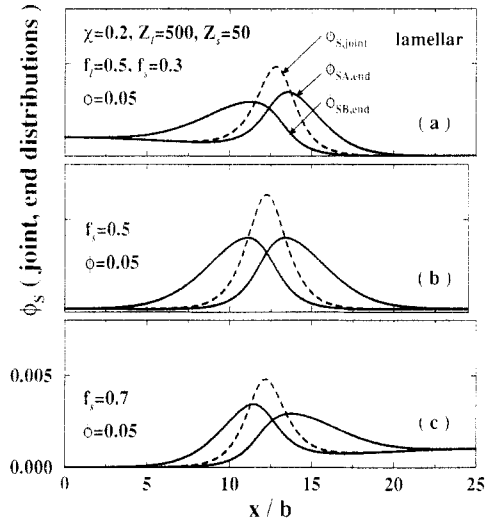

Figure 11. Calculated lamellar joint and end distributions of the short diblocks for $Z_l = 500$, $Z_s = 50$, and $f_l = 0.5$: (a) $\phi = 0.05$, $f_s = 0.3$, (b) $\phi = 0.05$, $f_s = 0.5$, and (c) $\phi = 0.05$, $f_s = 0.7$. The end distributions are plotted as solid lines, and the joint distribution is plotted as dashed lines. Changes in the lengths of the horizontal axes correspond to the changes in the domain size with added short chains.

the adjacent domain. The different box sizes indicate different amounts of shrinkage of the domain size as short diblocks of different compositions are added to the long diblocks. We have not shown the profiles for $f_s \simeq 0.95$ (homopolymer filler region), for which case the domain size increases. Figure 9a shows the clean domain boundary interface, which is very similar to a homopolymer–homopolymer interface. Figure 9c shows the symmetric–symmetric combination, with almost all of the short diblocks located at the interface and the largest reduction in the domain size. Figure 9b,d shows a smaller reduction in the domain size than Figure 9c, but, more importantly, demonstrates that the composition ratio of the short

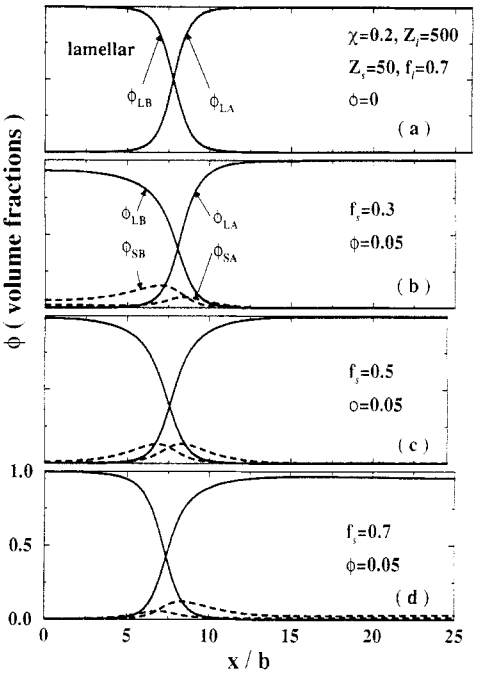

Figure 12. Calculated lamellar concentration profiles for $Z_l = 500$, $Z_s = 50$, and $f_l = 0.7$: (a) $\phi = 0$, (b) $\phi = 0.05$, $f_s = 0.3$, (c) $\phi = 0.05$, $f_s = 0.5$, and (d) $\phi = 0.05$, $f_s = 0.7$. The long chain profiles are plotted as solid lines, and the short chain profiles are plotted as dashed lines. Changes in the lengths of the horizontal axes correspond to the changes in the domain size with added short chains.

diblocks affects the amount of material localized at the domain boundary interface. This is consistent with the limiting situation where for $f_s \simeq 0$ or $f_s \simeq 1$ none of the short diblocks localize at the interface, and they act as fillers in the bulk of the domains. Figure 10c,d shows that the distribution functions for the joints and ends of the long diblocks are affected very little by the addition of a small amount of short diblocks of different compositions. However, the calculated end profiles, rising gradually from the center of the domain interface to a flat maximum at the middle of the domain, do not agree with the analytical predictions based on the strong segregation theory of Semenov, which predicts a steeper rise of the end distributions at the middle of the domain ($\propto x/(d^2-x^2)^{1/2}$).[8] This is interesting because it shows that even though we are in the strong segregation regime ($\chi Z = 100$), we are still far from the large Z limit where Semenov's theory applies. Figure 11a–c for the end and joint distributions of the short diblocks emphasize the delocalization effect of the asymmetry in the short diblock composition ratio.

Figures 12–14 show the density profiles and end and joint distribution functions for highly asymmetric large diblocks assembled into a lamellar phase, with and without added short diblocks of different composition ratios. The cylindrical structure is, in fact, the stable structure in this case, and the corresponding plots are shown in Figures 15–17. We will compare the results for the two structures. Figure 12a,c shows that, as far as the domain boundary interface is concerned, there is little difference for the asymmetric long diblock, symmetric short diblock profiles from the symmetric–symmetric profiles displayed in Figure 9a,c. For opposing asymmetries ($f_l = 0.7$, $f_s = 0.3$), Figure 12b shows more delocalization of the short diblock from the interface than in Figure 9b and also more delocalization than for identical asymmetries ($f_l = 0.7$, $f_s = 0.7$) shown in Figure 12d. Figure 13a–d shows the effect of packing short blocks into a small linear domain, and Figure 14a–c emphasizes the effects of identical and opposing asymmetries shown in Figure 12b,d.

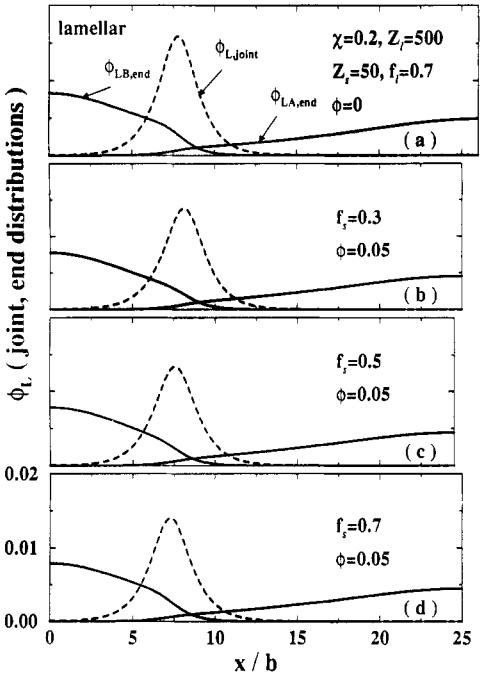

Figure 13. Calculated lamellar joint and end distributions of the long diblocks for $Z_l = 500$, $Z_s = 50$, $f_l = 0.7$: (a) $\phi = 0$, (b) $\phi = 0.05$, $f_s = 0.3$, (c) $\phi = 0.05$, $f_s = 0.5$, and (d) $\phi = 0.05$, $f_s = 0.7$. The end distributions are plotted as solid lines, and the joint distribution is plotted as dashed lines. Changes in the lengths of the horizontal axes correspond to the changes in the domain size with added short chains.

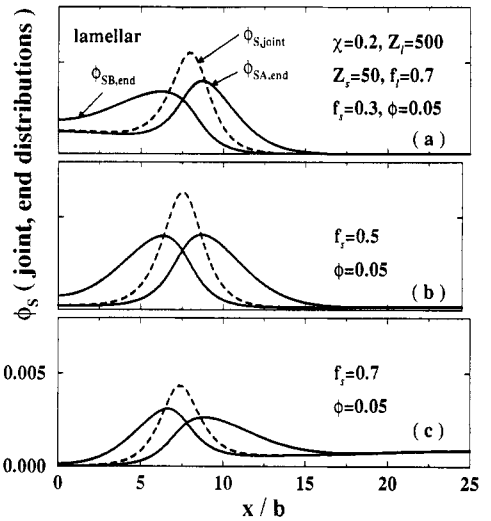

Figure 14. Calculated lamellar joint and end distributions of the short diblocks for $Z_l = 500$, $Z_s = 50$, and $f_l = 0.7$: (a) $\phi = 0.05$, $f_s = 0.3$, (b) $\phi = 0.05$, $f_s = 0.5$, and (c) $\phi = 0.05$, $f_s = 0.7$. The end distributions are plotted as solid lines, and the joint distribution is plotted as dashed lines. Changes in the lengths of the horizontal axes correspond to the changes in the domain size with added short chains.

Figure 15b, for the cylindrical phase with opposing asymmetries ($f_l = 0.7$, $f_s = 0.3$), indicates the largest delocalization of short diblocks from the interface of all the profiles shown. Figures 15–17 have the drawback that only a single plane of a two-dimensional profile structure can be shown. Nevertheless, these profiles (particularly Figure 16) show that the short blocks of the long molecules can now be packed into a larger volume per chain in the cylindrical phase than in the lamellar phase, resulting in a lower packing free energy and stabilizing the cylindrical phase. Figure 17a,c shows the large difference in delocalization of the short diblock when the composition symmetries are opposite ($f_l = 0.7$, $f_s = 0.3$) and identical

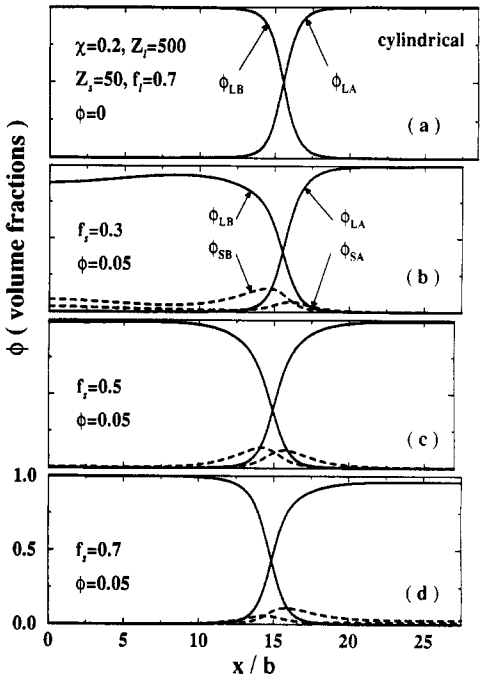

Figure 15. Calculated cylindrical concentration profiles for $Z_l = 500$, $Z_s = 50$, and $f_l = 0.7$: (a) $\phi = 0$, (b) $\phi = 0.05$, $f_s = 0.3$, (c) $\phi = 0.05$, $f_s = 0.5$, and (d) $\phi = 0.05$, $f_s = 0.7$. The long chain profiles are plotted as solid lines, and the short chain profiles are plotted as dashed lines. Changes in the lengths of the horizontal axes correspond to the changes in the domain size with added short chains.

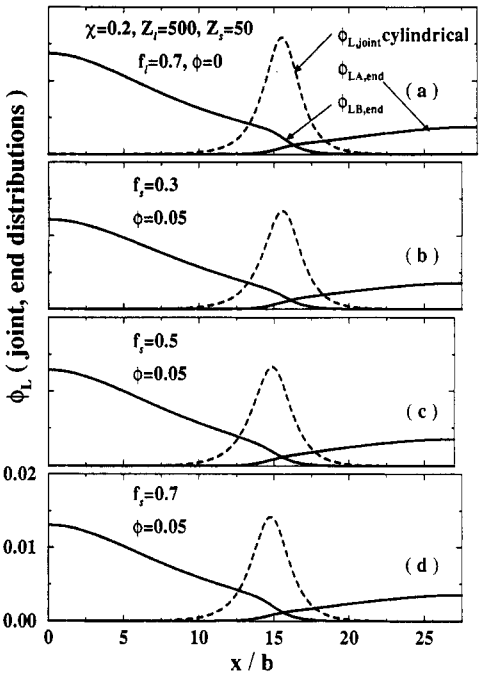

Figure 16. Calculated cylindrical joint and end distributions of the long diblocks for $Z_l = 500$, $Z_s = 50$, and $f_l = 0.7$: (a) $\phi = 0$, (b) $\phi = 0.05$, $f_s = 0.3$, (c) $\phi = 0.05$, $f_s = 0.5$, and (d) $\phi = 0.05$, $f_s = 0.7$. The end distributions are plotted as solid lines, and the joint distribution is plotted as dashed lines. Changes in the lengths of the horizontal axes correspond to the changes in the domain size with added short chains.

($f_l = 0.7$, $f_s = 0.7$). Figure 17b shows the asymmetry at the domain interface for symmetric short diblocks, arising from the interfacial curvature of the two-dimensional cylindrical phase.

4. Discussion

Using the approach developed by Hong and Noolandi,[11] we have derived the mean-field equations for a system

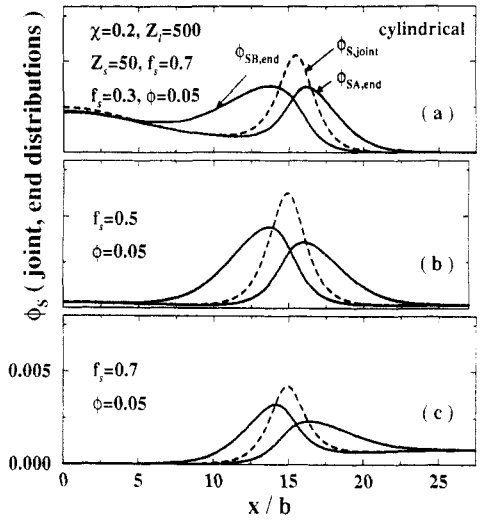

Figure 17. Calculated cylindrical joint and end distributions of the short diblocks for $Z_l = 500$, $Z_s = 50$, and $f_l = 0.7$: (a) $\phi = 0.05$, $f_s = 0.3$, (b) $\phi = 0.05$, $f_s = 0.5$, and (c) $\phi = 0.05$, $f_s = 0.7$. The end distributions are plotted as solid lines, and the joint distribution is plotted as dashed lines. Changes in the lengths of the horizontal axes correspond to the changes in the domain size with added short chains.

consisting of two diblock copolymers. These equations were solved numerically for the distribution functions, density profiles, and the associated free energies. These mean-field results are used to construct the phase diagrams of the system, which demonstrate that the short copolymer chains have surprisingly large effects on the phase diagram of the system. Under appropriate conditions (*e.g.*, $f_s \simeq 0.35$ and $\phi = 0.05$), the short chains are able to change the topology of the phase diagram in the sense that the spherical structure is absent (Figure 7). We argue that, depending on the short diblock composition f_s, there are two mechanisms driving the changes in the phase diagram. When f_s is close to 0 or 1, most of the short diblocks remain in the bulk domains, and the short chains act like homopolymer fillers. On the other hand, when f_s is close to 0.5, a substantial volume fraction of the short diblocks (up to about 20%) segregate to the interfaces and behave as compatibilizers, affecting the local interfacial curvature according to their composition ratio. The effect on the density profiles (see Figure 2), which is of interest for experimentalists using neutron reflectivity techniques,[12] is even larger.

In the cases where $f_s \simeq 0$ or $f_s \simeq 1$, the effects of the short chains are mainly on the filling of the corresponding domains, resulting in a decrease of the stretching free energy. On the other hand, there is little effect of these short chains on the interfacial properties; thus we expect that no change in the interfacial tension. The combined effect of these two mechanisms is an increase in the equilibrium domain size.

In the cases where $f_s \simeq 0.5$, there is strong segregation of the short chains to the interfaces. The effects of the short chains at the interfaces are 2-fold: a reduction of the interfacial tension and an increase of the stretching free energy. Both effects favor a decrease in the equilibrium domain sizes. When these two effects cancel on a phase boundary, we have a structural fixed point, which we denote by (f_l, f_s^*). Considering the right-hand side of the phase diagrams in Figures 6 and 7 ($f_l > 0.5$), for $f_s > f_s^*$ small amounts of added short diblocks destabilize the phases with larger interfacial curvatures, and for $f_s < f_s^*$ small amounts of added short diblocks stabilize the phases with smaller interfacial curvatures. Similar arguments hold for the left-hand side of the phase diagrams ($f_l < 0.5$) when we interchange f_s with $1 - f_s$. Since the existence of structural fixed points is based on symmetry arguments, we expect this prediction to be generally valid beyond mean-field theory.

Acknowledgment. We thank Dr. Chuck Yeung for many useful discussions. This work is supported in part by the Natural Sciences and Engineering Research Council of Canada.

6. Appendix

1. Mean-Field Theory. We consider mixtures of two types (long and short) of diblock copolymer chains. The two copolymers are chemically identical and differ only in their degrees of polymerization and compositions. We denote the degrees of polymerization of the copolymers as Z_{ip}, where $i = 1, 2$ labels the chain type (long and short chains) and $p = A, B$ labels the blocks; thus $Z_i = Z_{iA} + Z_{iB}$ is the degree of polymerization of the ith type ($Z_1 = Z_l$, $Z_2 = Z_s$, and $Z_l > Z_s$). We assume that there are n_l long diblock copolymer chains and n_s short diblock copolymer chains in a finite volume V. Starting from the usual Edwards Hamiltonian and following the procedure of Hong and Noolandi,[11] we can derive the free energy density of the system within mean-field theory. The free energy per unit volume has the form

$$f \equiv \frac{F}{\rho_0 V k_B T} = f_H + \Delta f \tag{A1}$$

where

$$f_H = \chi \bar{\phi}_A \bar{\phi}_B + \left[\frac{\bar{\phi}_1}{Z_l} \ln \frac{\bar{\phi}_1}{Z_l} + \mu_{01}\bar{\phi}_1\right] + \left[\frac{\bar{\phi}_2}{Z_s} \ln \frac{\bar{\phi}_2}{Z_s} + \mu_{02}\bar{\phi}_2\right] \tag{A2}$$

is the free energy density for a homogeneous phase. The total block volume fractions are $\bar{\phi}_p = \bar{\phi}_{1p} + \bar{\phi}_{2p}$, and the total chain volume fractions are $\bar{\phi}_i = \bar{\phi}_{iA} + \bar{\phi}_{iB}$. Here $\bar{\phi}_{ip} = n_i Z_{ip}/\rho_0 V$ is the volume fraction of the ip component in the homogeneous phase, χ is the Flory–Huggins interaction parameter, ρ_0 is a reference density, and the μ_{0i} are constants. We have also assumed that the density of the pure materials ρ_{0p} is the same as ρ_0. Note that for a given set of parameters, f_H is a constant. Also, the incompressibility condition requires

$$\sum_{i,p} \bar{\phi}_{ip} = 1 \tag{A3}$$

We use the notation that $\phi \equiv \bar{\phi}_2$ is the total volume fraction of the short chains in the melt. The molecular structure of the chains is specified by two parameters,

$$f_l = \frac{Z_{1A}}{Z_l}$$

$$f_s = \frac{Z_{2A}}{Z_s} \tag{A4}$$

which specify the compositions of the long and short diblocks, respectively. The system is completely defined by the set of parameters $\{\chi, Z_l, Z_s, f_l, f_s, \phi\}$. In terms of these parameters, the volume fractions in the homogeneous phase (the reference state) are

$$\bar{\phi}_A = (1 - \phi) f_l + \phi f_s$$

$$\bar{\phi}_B = 1 - (1 - \phi)f_l - \phi f_s$$

The free energy density due to the inhomogeneities of the system is

$$\Delta f = \frac{1}{V}\int d\mathbf{r}\chi\,[\phi_A(\mathbf{r})\phi_B(\mathbf{r}) - \bar{\phi}_A\bar{\phi}_B] - \frac{1}{V}\int d\mathbf{r}[\omega_A(\mathbf{r})\phi_A(\mathbf{r}) + \omega_B(\mathbf{r})\phi_B(\mathbf{r})] - \frac{1-\phi}{Z_l}\ln Q_l - \frac{\phi}{Z_s}\ln Q_2 \quad \text{(A5)}$$

where the concentrations are

$$\phi_A(\mathbf{r}) = \phi_{1A}(\mathbf{r}) + \phi_{2B}(\mathbf{r})$$

$$\phi_B(\mathbf{r}) = \phi_{1A}(\mathbf{r}) + \phi_{2B}(\mathbf{r})$$

and, within the mean-field approximation, the block concentrations $\phi_{ip}(\mathbf{r})$ are given by

$$\phi_{iA}(\mathbf{r}) = \frac{\phi_{iA}}{Z_{iA}Q_i}\int_0^{Z_{iA}} dt q_{CA}(\mathbf{r}, t)q^i{}_{AB}(\mathbf{r}, Z_{iA} - t)$$

$$\phi_{iB}(\mathbf{r}) = \frac{\phi_{iB}}{Z_{iB}Q_i}\int_0^{Z_{iB}} dt q_{CB}(\mathbf{r}, t)q^i{}_{BA}(\mathbf{r}, Z_{iB} - t) \quad \text{(A6)}$$

The quantity Q_i is given by

$$Q_i = \frac{1}{V}\int d\mathbf{r}q^i{}_{AB}(\mathbf{r}, Z_{iA}) = \frac{1}{V}\int d\mathbf{r}q^i{}_{BA}(\mathbf{r}, Z_{iB}) \quad \text{(A7)}$$

In these expressions, the functions $q_{CA}(\mathbf{r}, t)$, $q_{CB}(\mathbf{r}, t)$, $q_{AB}(\mathbf{r}, t)$, and $q_{BA}(\mathbf{r}, t)$ are the end-integrated distribution functions for the diblock copolymer chains.[5] These functions are the solutions of the modified diffusion equations:

$$\frac{\partial}{\partial t}q_{CA}(\mathbf{r}, t) = \frac{b^2{}_A}{6}\nabla^2 q_{CA}(\mathbf{r}, t) - \omega_A(\mathbf{r})q_{CA}(\mathbf{r}, t)$$

$$\frac{\partial}{\partial t}q_{CB}(\mathbf{r}, t) = \frac{b^2{}_B}{6}\nabla^2 q_{CB}(\mathbf{r}, t) - \omega_B(\mathbf{r})q_{CB}(\mathbf{r}, t)$$

$$\frac{\partial}{\partial t}q^i{}_{AB}(\mathbf{r}, t) = \frac{b^2{}_A}{6}\nabla^2 q^i{}_{AB}(\mathbf{r}, t) - \omega_A(\mathbf{r})q^i{}_{AB}(\mathbf{r}, t)$$

$$\frac{\partial}{\partial t}q^i{}_{BA}(\mathbf{r}, t) = \frac{b^2{}_B}{6}\nabla^2 q^i{}_{BA}(\mathbf{r}, t) - \omega_B(\mathbf{r})q^i{}_{BA}(\mathbf{r}, t) \quad \text{(A8)}$$

The initial conditions for the q's are

$$q_{CA}(\mathbf{r}, 0) = 1$$

$$q_{CB}(\mathbf{r}, 0) = 1$$

$$q^i{}_{AB}(\mathbf{r}, 0) = q_{CB}(\mathbf{r}, Z_{iB})$$

$$q^i{}_{BA}(\mathbf{r}, 0) = q_{CA}(\mathbf{r}, Z_{iA}) \quad \text{(A9)}$$

The mean-fields $\omega_p(\mathbf{r})$ are to be obtained self-consistently from

$$\omega_A(\mathbf{r}) = \chi[\phi_B(\mathbf{r}) - \phi_B] + \eta(\mathbf{r})$$

$$\omega_B(\mathbf{r}) = \chi[\phi_A(\mathbf{r}) - \phi_B] + \eta(\mathbf{r}) \quad \text{(A10)}$$

where $\eta(\mathbf{r})$ is to be adjusted to ensure at the incompressibility condition

$$\phi_A(\mathbf{r}) + \phi_B(\mathbf{r}) = 1 \quad \text{(A11)}$$

Because of the mean-field approximation, there are only two independent mean-fields $\omega_A(x)$ and $\omega_B(x)$ despite the fact that the system contains two types of copolymer chains. We also note that the free energy and the density profiles do not depend on a constant shift of the mean fields. In the calculations we report here, we use the convention that the average values of the mean fields are zero

$$\int_V d\mathbf{r}\omega_p(\mathbf{r}) = 0$$

For each microphase considered, the system is assumed to form an infinite periodic structure, described by a set of lattice vectors and an associated unit cell of volume Ω. For each system we perform a series of self-consistent calculations to determine the equilibrium microstructure, corresponding lattice parameters, and the free energy. In the lamellar structure, the problem is one-dimensional, and the lattice parameter coincides with the domain size d. For the cylindrical and spherical structures, we approximate the unit cell by a cylinder or a sphere which contains one domain, with its radius denoted by d. We solve the modified diffusion equations in the domain $[0, d]$ and exploit the fact that the central plane of every domain is a plane of symmetry; thus the derivatives of the propagators vanish at $x = 0$ and $x = d$.

2. Computational Algorithm. We implement the mean-field theory for the binary diblock copolymer melts as follows:

1. For each set of values of $\{\chi, Z_l, Z_s, f_l, f_s, \phi\}$, we determine the values of $\bar{\phi}_A$, $\bar{\phi}_B$.

2. For a given domain size d, we make an initial guess for the mean-fields $\omega_A(x)$ and $\omega_B(x)$. The initial values of the $\omega_{A,B}$ are calculated from eq A10 by assuming $\eta(x) = 0$ and a hyperbolic tangent profile for the densities. It turns out that the final results do not depend on the initial mean fields, but an appropriate choice of the ω's will speed up the computation.

3. Using the $\omega_{A,B}(x)$, we solve the modified diffusion equations (eq A8) with the appropriate initial conditions and boundary conditions. These propagators are then used to compute the densities $\phi_{ip}(x)$.

4. For the given mean-fields $\omega_{A,B}(x)$, we obtain the values of $\eta(x)$ by using eq A10

$$\eta(x) = [\omega_A(x) + \omega_B(x)]/2$$

5. For the newly obtained $\eta(x)$ and $\phi_{ip}(x)$, we use eq A10 to calculate a new guess for the mean fields $\omega'_{A,B}(x)$. It is found that we can enhance the convergence by adding an extra term to push the potentials toward incompressibility. We define

$$\omega''_{A,B}(x) = \omega'_{A,B}(x) - \alpha[1 - \sum_{ip}\phi_{ip}(x)]$$

where $0 \le \alpha \le 1$.

6. For the given $\omega''_{A,B}(x)$, we make the next guess for $\omega_{A,B}(x)$ either using

$$\omega_p(x) \rightarrow \omega_p(x) + \delta(\omega''_p(x) - \omega_p(x))$$

or using the modified secant method. In practice it is

found that the convergence is enhanced by switching from one method to the other in the iteration process.

7. Return to step (3) with the new guess for $\omega_p(x)$ and continue until convergence is reached and incompressibility is achieved. We require that the maximum values of $|1 - \sum_{ip}\phi_{ip}(x)|$ and $|\omega_p(x) - \omega'_p(x)|$ are less than 10^{-6}.

The calculation was repeated for different values of the domain size d. We use the values $Z_l = 500$, $Z_s = 50$, and $\chi = 0.2$ for most of the calculations reported here. For the pure long diblock copolymer melts, $\chi Z_l = 100$; thus the system is clearly in the strong segregation limit. The values of the total volume fractions of the short chains ranged from $\phi = 0.00$ to 0.05. We also set the length scale in terms of the Kuhn length $b = b_A = b_B = 1$. The modified diffusion equations (eq A8) were integrated using the Crank–Nicholson method with $dt = Z_{ip}/400$ and $dx = d/100$.

References and Notes

(1) Bates, F. S. *Science* **1991**, *151*, 898.
(2) Shibayama, M.; Hashimoto, T.; Kawai, H. *Macromolecules* **1983**, *16*, 16.
(3) Thomas, E. L.; Anderson, D. M.; Henkee, C. S.; Hoffman, D. *Nature* **1988**, *334*, 598.
(4) Hasegawa, H.; Tanaka, H.; Yamasaki, K.; Hashimoto, T. *Macromolecules* **1987**, *20*, 1651.
(5) Noolandi, J.; Hong, K. M. *Macromolecules* **1982**, *15*, 482.
(6) De Gennes, P.-G. *Solid State Physics, Supplement 14*; Academic Press, New York; 1978; p 1.
(7) Helfand, E.; Wasserman, W. R. *Macromolecules* **1976**, *9*, 879.
(8) Semenov, A. N. *Sov. Phys. JETP* **1985**, *61*, 733.
(9) Helfand, E.; Wasserman, W. R. *Macromolecules* **1980**, *13*, 994.
(10) Helfand, E.; Wasserman, W. R. *Macromolecules* **1978**, *11*, 969.
(11) Hong, K. M.; Noolandi, J. *Macromolecules* **1981**, *14*, 727.
(12) Russell, T. P. *Mater. Sci. Rep.* **1990**, *5*, 171.